Magnetic Ordering in Ho-doped Bi_2Te_3 Topological Insulator Thin Films

A. I. Figueroa,[1] S. E. Harrison,[2,3] L. J. Collins-McIntyre,[2] G. van der Laan,[1] and T. Hesjedal[2,*]

[1] *Magnetic Spectroscopy Group, Diamond Light Source, Didcot, OX11 0DE, United Kingdom*
[2] *Department of Physics, Clarendon Laboratory, University of Oxford, Oxford, OX1 3PU, United Kingdom*
[3] *Department of Electrical Engineering, Stanford University, Stanford, California 94305, USA*

(Dated: April 6, 2016)

We investigate the magnetic properties of Ho-doped Bi_2Te_3 thin films grown by molecular beam epitaxy. Analysis of the polarized x-ray absorption spectra at the Ho M_5 absorption edge gives an effective $4f$ magnetic moment which is ∼45% of the Hund's rule ground state value. X-ray magnetic circular dichroism (XMCD) shows no significant anisotropy, which suggests that the reduced spin moment is not due to the crystal field effects, but rather the presence of non-magnetic or antiferromagnetic Ho sites. Extrapolating the temperature dependence of the XMCD measured in total electron yield and fluorescence yield mode in a field of 7 T gives a Curie-Weiss temperature of $\theta_{CW} \approx -30$ K, which suggests antiferromagnetic ordering, in contrast to the paramagnetic behavior observed with SQUID magnetometry. From the anomaly of the XMCD signal at low temperatures, a Néel temperature T_N between 10 K and 25 K is estimated.

PACS numbers: 75.30.Hx; 78.70.Dm; 75.50.Pp; 73.61.Ng

I. INTRODUCTION

Topological insulators (TIs)[1,2] have been at the center of interest for unlocking novel physical effects and spin-based electronics alike, owing to their unique electronic properties. The gapless topological surface state (TSS) of three-dimensional (3D) TIs, with its counter-propagating streams of oppositely spin-polarized electrons, is protected by time-reversal symmetry (TRS) against back-scattering thereby resulting in high mobilities. The quantum anomalous Hall effect (QAHE), which has been observed in magnetic TIs,[3] is one such effect where quantized transport occurs in the absence of an external magnetic field and thus discrete Landau levels. The key ingredient for observing the QAHE is the opening of a band gap in the band structure of the TSS, e.g., via magnetic doping. In the prototypical 3D TIs of the $(Bi,Sb)_2(Se,Te)_3$ type,[4] doping with $3d$ transition metals, such as Mn and Cr,[5–7] has been successful for achieving ferromagnetically ordered TIs. It is further essential to achieve the ferromagnetic state without an increase of the bulk carrier density, as has been achieved for $Cr_{0.15}(Bi_{0.1}Sb_{0.9})_{1.85}Te_3$ with a T_C of 16 K.[8]

In general, however, doping with transition metals has the intrinsic disadvantage that a divalent ion replaces the trivalent Bi due to hybridization, as it was shown for Cr doping of Bi_2Se_3.[9] Doping with rare-earth elements, on the other hand, leads to an isoelectronic and substitutional doping on the Bi site.[10] Among them, $GdBiTe_3$ is particularly promising, as *ab-initio* calculations predicted ferromagnetic order and the existence of the QAHE.[11] Unfortunately, the solubility limit for Gd doping in Bi_2Te_3 bulk crystals is very low, between ∼1-5%.[12] Gd-doped Bi_2Te_3 bulk crystals with low doping concentrations have been reported to be either paramagnetic[12] or weakly antiferromagnetic.[13] In thin films, this limit can be significantly increased to ∼40%, still short of the required 1:1 ratio of Gd:Bi.[14] Magnetic measurements revealed that the moment is independent of the doping level and that the films are paramagnetic.[15]

In contrast to the ferromagnetic TIs, antiferromagnetic TIs are an intriguing oddity as they both break translational symmetry, which TIs are known not to do, and TRS, yet preserve the $\mathbb{Z}_2$ topological invariant by the combination of both.[16] They offer unique advantages such as creating spin-orbit coupling effects which are absent in the nonmagnetic phase, as it has been shown for the example of the half-Heusler alloy GdBiPt, leading quantized Hall conductance and magnetoelectric effects as well.[17] Kim *et al.* reported the successful antiferromagnetic doping of Bi_2Te_3 above a critical Gd doping concentration.[18] Using density functional theory calculations, the authors explain that the antiferromagnetic ordering is resulting from weak, indirect Gd-Te-Gd coupling.

Recently, we presented the growth of high-quality $(Ho_xBi_{1-x})_2Te_3$ thin films by molecular beam epitaxy (MBE) with high Ho concentrations up to $x = 0.21$. Details about the growth, structural investigations, as well as magnetic bulk properties can be found in Ref. 19. Angle-resolved photoemission spectroscopy confirmed the existence of the topological surface state in the band structure of the Ho-doped films, however, no magnetic doping-induced gap at the Dirac point has been observed.[19] Here, we address the open question of the magnetic surface properties of Ho-doped thin films using magnetic x-ray dichroism in the pursuit of an antiferromagnetic TI thin film system.

II. THIN FILM GROWTH, STRUCTURAL AND MAGNETIC BULK PROPERTIES

For the x-ray spectroscopic study of the magnetic properties of Ho-doped thin Bi_2Te_3 thin films, we focused on the highest quality film from the doping series reported

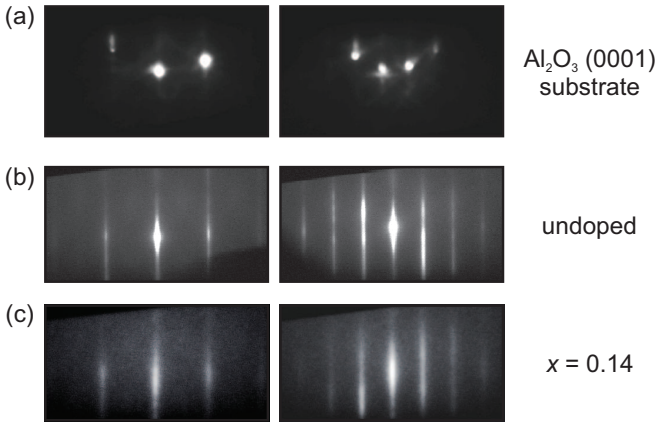

FIG. 1. (a) RHEED images for the Al_2O_3 (0001) substrate along the $[11\bar{2}0]$ (left column) and $[10\bar{1}0]$ (right column) azimuths, respectively. Corresponding RHEED patterns for (b) an undoped Bi_2Te_3 film and (c) the doped $x = 0.14$ film.

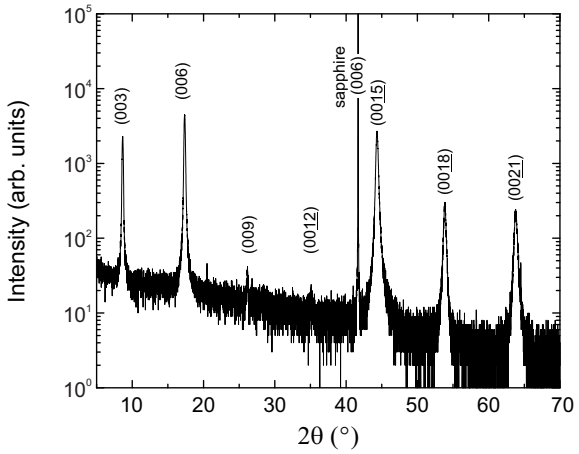

FIG. 2. XRD study. Symmetric $2\theta - \omega$ scan of the Ho-doped Bi_2Te_3 thin film sample ($x = 0.14$) on c-plane sapphire.

in Ref. 19. The 80-nm-thick film with a Ho concentration of $x = 0.14$ (5.5 at.-%) in $(Ho_xBi_{1-x})_2Te_3$ was grown on c-plane sapphire using MBE, closely following a recipe established for Dy- and Gd-doped Bi_2Te_3 thin film growth,[15,20] and as described in detail in Ref. 19. Figure 1 shows reflection high-energy electron diffraction (RHEED) images of the doped $x = 0.14$ film, along with an undoped Bi_2Te_3 film and the Al_2O_3 (0001) substrate for comparison. The RHEED patterns of the doped and undoped films have the same streaky features, representative of a flat surface morphology. The patterns repeat upon 60° azimuthal rotation, as expected from a twinned crystal of the $R\bar{3}m$ space group. The doped film has the same rhombohedral crystal structure as Bi_2Te_3, as can be seen in the x-ray diffraction (XRD) spectrum [Fig. 2] which only shows the sapphire (006) and the $(00\underline{l})$ film peaks. No secondary phases are found in this spectrum. The doped sample has a smaller c-axis lattice constant (30.39 Å) as compared to the undoped sample (30.61 Å), and shows some degree of peak broadening. The summed cation to anion ratio, as determined by Rutherford backscattering spectrometry (RBS) and particle-induced x-ray emission (PIXE), is 2:3 and indicative of substitutional Ho doping on Bi sites.[19]

The magnetic (bulk) property measurement of the Ho-doped film shows paramagnetic behavior down to 2 K and a saturation moment of $\sim(5.14\pm0.65)$ μ_B/Ho, which is half of the theoretical maximum effective moment.[19] The moment saturates at $\sim$4 T at a temperature of 2 K. In LS-coupling, the Hund's rule ground state $^5I_8$ has spin, orbital, and total angular momenta, $S = 2$, $L = 6$, and $J = 8$. Using the Landé splitting factor, $g_J = 3/2 + [S(S+1) - L(L-1)]/[2J(J+1)]$ this gives an effective magnetic $4f$ moment, $\mu_{\text{eff}} = g_J\sqrt{J(J+1)}$ = 10.61 μ_B/Ho. Note that the magnetic behavior of Ho-doped films is different from Gd-doped films where the full spin moment was observed,[15] and also different from Dy-doped films, where the moment was found to be doping concentration-dependent, with an increase at lower doping concentrations.[20] The plot of the inverse susceptibility, $1/\chi$, follows the Curie-Weiss law, where a Weiss temperature of $\theta_{\text{CW}} = -0.8$ K was found. The experimentally determined $\sim$50% reduced magnetic moment, which could be explained by a number of causes such as dopant oxidation, crystal-field effects, or antiferromagnetic ordering,[16,18] motivated our x-rays spectroscopic study that is presented in Sec. III.

III. X-RAY MAGNETIC CIRCULAR DICHROISM

The element-specific technique of XMCD is used to probe the local electronic character of the magnetic ground state.[21–23] This technique allows an unambiguous determination of the electronic and magnetic state of transition-metal and rare-earth dopants in TIs.[5,15,20,24,25]

Experimental. X-ray absorption spectra (XAS) at the Ho M_5 edge were measured at different temperatures down to 2.5 K on beamline I10 at the Diamond Light Source using a UHV compatible 14 T superconducting magnet with a liquid He cooled variable temperature insert.[23] XAS measurements were made simultaneously in total-electron-yield (TEY) and fluorescence-yield (FY) mode. The XMCD is obtained from the difference between two XAS spectra recorded with the x-ray helicity vector and applied magnetic field antiparallel and parallel, respectively. The magnetic field is along the x-ray beam and the samples (with the normal $\parallel$ c-axis) were measured at both normal ($\theta = 0°$) and grazing ($\theta = 75°$) incidence. The XMCD is obtained by reversing the polarization of the incident x-rays to avoid having to change the magnetic field of the superconducting magnet. X-ray magnetic linear dichroism measurements, which are well-suited for the study of antiferromagnetic materials,[26] were performed as well, however, due to the crystal field

contribution did not yield conclusive results.

Determination of magnetic moment. While in principle sum-rule analysis[27–29] can be used to obtain the magnetic moment in rare earths, the large jj mixing between the $3d_{5/2}$ and $3d_{3/2}$ core levels necessitates a correction factor to extract the spin moment, compared to the late $3d$ transition metals. Two alternative methods, namely (i) fitting the experimental spectra with the three polarization components and (ii) using the peak asymmetry, $(I_L - I_R)/(I_L + I_R)$, were used and the details are described in Ref. 30. They both make use of the fact that in rare earths the spin and orbital moments are parallel and both methods give very similar results.

The obtained XMCD intensities at 2.5 K are equal to 45% and 46.5%, for normal and grazing incidence, respectively, of the calculated value for the Hund's rule state.[30] The effective magnetic moment is therefore $\mu_{\text{eff}} \approx 4.85\ \mu_{\text{B}}$/Ho. The 'missing' intensity in the polarized spectra is due to non-magnetic or antiferromagnetic Ho sites. Oxidation is a possible cause and, since it can be assumed that it starts at the surface, should be detectable by comparing surface sensitive TEY detection having a sampling depth of 6 nm with bulk-sensitive FY detection.[23,31]

Temperature dependence of the Ho XMCD. Figure 3(a) shows the trend in the Ho magnetic moment, extracted from the XMCD as a function of temperature for both FY and TEY, which were measured simultaneously. The Ho M_5 XMCD for the $x = 0.14$ sample, shown in the inset, was measured over a range of temperatures with out-of-plane applied field of 7 T. The moment is zero at 300 K, and gradually increases for decreasing temperature. It reaches a maximum around 7 K, after which it reduces again going further down in temperature. This is in stark contrast with SQUID measurements on Ho-doped samples, which showed paramagnetic bulk behavior down to 2 K.[19] Note that the diamagnetic signal from the substrate does not contribute to the Ho XMCD and that this is one of the reasons the low temperature deviation in the magnetization is evident in XMCD but not in SQUID measurements. An estimation of the Curie temperature may be obtained by plotting the inverse of the magnetic susceptibility $1/\chi = H/M$ (using the moment $\langle M \rangle$ obtained from XMCD) as a function of temperature [Fig. 3(b)]. This shows the typical linear dependency expected for a paramagnetic system with a small deviation at lower temperatures. Linear extrapolation leads to an estimated Curie-Weiss temperature $\theta_{\text{CW}} \approx -30$ K. The Néel temperature T_{N} can only be estimated to be in a range between 10 and 25 K due to a lack of data points in that temperature range. From the fit to the data points below 25 K, T_{N} is ∼22 K.

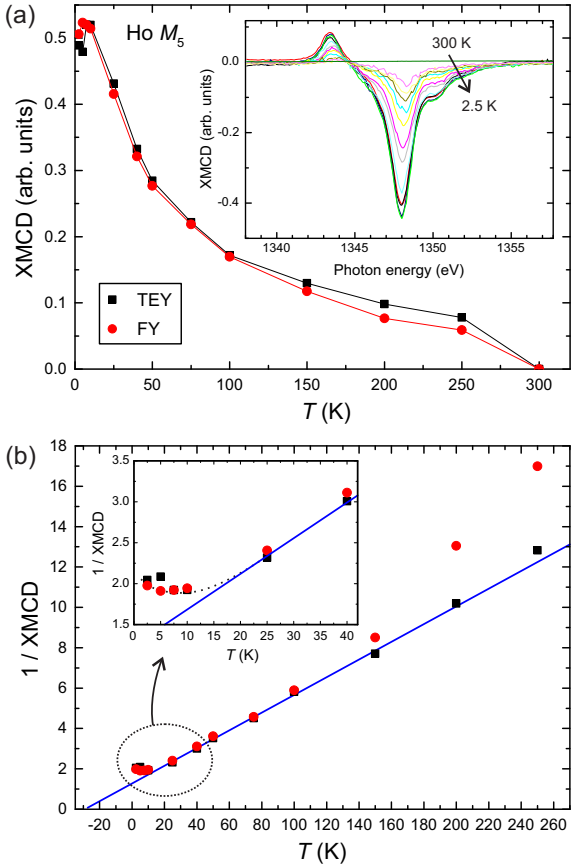

FIG. 3. Temperature dependent XMCD measurements of the $x = 0.14$ Ho-doped Bi_2Te_3 thin film. (a) Magnetic moment as a function of temperature extracted from the Ho M_5 XMCD measured in total-electron yield (TEY) at normal incidence in applied field of 7 T shown in the inset.[19] (b) Inverse susceptibility derived from the XMCD signal. The blue straight line through the TEY XMCD suggests a Curie-Weiss temperature of $\theta_{\text{CW}} \approx -30$ K. The inset shows the anomaly at low temperatures where the inverse susceptibility increases with decreasing temperature. The fluorescence yield (FY) (black squares) and TEY were measured simultaneously.

IV. SUMMARY AND CONCLUSIONS

We presented a study of the magnetic state of high-quality MBE-grown Ho-doped Bi_2Te_3 films. Ho M_5 XMCD-TEY measurements at 2.5 K give an effective magnetic moment of 45% of the Hund's rule value. The moment is maximum at ∼7 K for both FY and TEY. Extrapolating the temperature dependence of the XMCD measured in TEY in a field of 7 T gives a $\theta_{\text{CW}} = -30$ K. These results are clear evidence of antiferromagnetic ordering of Ho in Bi_2Te_3. This contribution is too small to be visible in bulk-sensitive SQUID magnetometry of the films. Future investigations are aimed at exploring the difference between the spectroscopic data and the bulk magnetometry measurements, which could point towards an involvement of the TSS in the magnetic coupling mechanism.

ACKNOWLEDGMENTS

Diamond Light Source is acknowledged for beamtime allocated on beamline I10 (proposal SI-10207). This publication arises from research funded by the John Fell Oxford University Press (OUP) Research Fund and the Research Complex at Harwell is acknowledged for their hospitality. SEH acknowledges partial financial support from a DARPA MESO Project (No. N66001-11-1-4105) and the VPGE (Stanford University) and LCM partial financial support from EPSRC (UK) through a Doctoral Training Award.

---

* Corresponding author: Thorsten.Hesjedal@physics.ox.ac.uk

[1] C. Kane and E. Mele, Phys. Rev. Lett. **95**, 146802 (2005).

[2] B. A. Bernevig, T. L. Hughes, and S.-C. Zhang, Science **314**, 1757 (2006).

[3] C.-Z. Chang, J. Zhang, X. Feng, J. Shen, Z. Zhang, M. Guo, K. Li, Y. Ou, P. Wei, L.-L. Wang, Z.-Q. Ji, Y. Feng, S. Ji, X. Chen, J. Jia, X. Dai, Z. Fang, S.-C. Zhang, K. He, Y. Wang, L. Lu, X.-C. Ma, and Q.-K. Xue, Science **340**, 167 (2013).

[4] Y. Xia, D. Qian, D. Hsieh, L. Wray, A. Pal, H. Lin, A. Bansil, D. Grauer, Y. S. Hor, R. J. Cava, and M. Z. Hasan, Nature Phys. **5**, 398 (2009).

[5] L. J. Collins-McIntyre, M. D. Watson, A. A. Baker, S. L. Zhang, A. I. Coldea, S. E. Harrison, A. Pushp, A. J. Kellock, S. S. P. Parkin, G. van der Laan, and T. Hesjedal, AIP Advances **4**, 127136 (2014).

[6] L. J. Collins-McIntyre, S. E. Harrison, P. Schoenherr, N.-J. Steinke, C. J. Kinane, T. R. Charlton, D. Alba-Veneroa, A. Pushp, A. J. Kellock, S. S. P. Parkin, J. S. Harris, S. Langridge, G. van der Laan, and T. Hesjedal, Europhys. Lett. **107**, 57009 (2014).

[7] A. I. Figueroa, G. van der Laan, L. J. Collins-McIntyre, S.-L. Zhang, A. A. Baker, S. E. Harrison, P. Schoenherr, G. Cibin, and T. Hesjedal, Phys. Rev. B **90**, 134402 (2014).

[8] C. Z. Chang, J. S. Zhang, M. H. Liu, Z.-C. Zhang, and X. Feng, "Carrier-independent ferromagnetism and giant anomalous Hall effect in magnetic topological insulators," (2011), arXiv:1108.4754.

[9] A. I. Figueroa, G. van der Laan, L. J. Collins-McIntyre, S.-L. Zhang, A. A. Baker, S. E. Harrison, P. Schoenherr, G. Cibin, and T. Hesjedal, Phys. Rev. B **90**, 134402 (2014).

[10] A. I. Figueroa, G. van der Laan, S. E. Harrison, G. Cibin, and T. Hesjedal, Sci. Rep. , submitted (2016).

[11] H.-J. Zhang, X. Zhang, and Z.-C. Zhang, "Quantum anomalous Hall effect in magnetic topological insulator $GdBiTe_3$," (2011), arXiv:1108.4857.

[12] Y. R. Song, F. Yang, M.-Y. Yao, F. Zhu, L. Miao, J.-P. Xu, M.-X. Wang, H. Li, X. Yao, F. Ji, S. Qiao, Z. Sun, G. B. Zhang, B. Gao, C. Liu, D. Qian, C. L. Gao, and J.-F. Jia, Appl. Phys. Lett. **100**, 242403 (2012).

[13] M. Elkholdi, M. Averous, S. Charar, C. Fau, G. Brun, H. Ghoumaribouanani, and J. Deportes, Phys. Rev. B **49**, 1711 (1994).

[14] S. Li, S. Harrison, Y. Huo, A. Pushp, H. Yuan, B. Zhou, A. Kellock, S. Parkin, Y.-L. Chen, T. Hesjedal, and J. Harris, Appl. Phys. Lett. **102**, 242412 (2013).

[15] S. E. Harrison, L. J. Collins-McIntyre, S. Li, A. A. Baker, L. R. Shelford, Y. Huo, A. Pushp, S. S. P. Parkin, J. S. Harris, E. Arenholz, G. van der Laan, and T. Hesjedal, J. Appl. Phys. **115**, 023904 (2014).

[16] R. S. K. Mong, A. M. Essin, and J. E. Moore, Phys. Rev. B **81**, 245209 (2010).

[17] R. A. Müller, N. R. Lee-Hone, L. Lapointe, D. H. Ryan, T. Pereg-Barnea, A. D. Bianchi, Y. Mozharivskyj, and R. Flacau, Phys. Rev. B **90**, 041109(R) (2014).

[18] J. Kim, K. Lee, T. Takabatake, H. Kim, M. Kim, and M.-H. Jung, Sci. Rep. **5**, 10309 (2015).

[19] S. E. Harrison, L. J. Collins-McIntyre, S.-L. Zhang, A. A. Baker, A. I. Figueroa, A. J. Kellock, A. Pushp, S. S. P. Parkin, J. S. Harris, G. van der Laan, and T. Hesjedal, Appl. Phys. Lett. **107**, 182406 (2015).

[20] S. E. Harrison, L. J. Collins-McIntyre, S.-L. Zhang, A. A. Baker, A. I. Figueroa, A. J. Kellock, A. Pushp, S. S. P. Parkin, J. S. Harris, G. van der Laan, and T. Hesjedal, J. Phys.: Condens. Matter **27**, 245602 (2015).

[21] G. van der Laan and B. T. Thole, Phys. Rev. B **43**, 13401 (1991).

[22] G. van der Laan, J. Phys.: Conf. Ser. **430**, 012127 (2013).

[23] G. van der Laan and A. I. Figueroa, Coord. Chem. Rev. **277–278**, 95 (2014).

[24] L. R. Shelford, T. Hesjedal, L. J. Collins-McIntyre, S. S. Dhesi, F. Maccherozzi, and G. van der Laan, Phys. Rev. B **86**, 081304 (2012).

[25] M. Watson, L. J. Collins-McIntyre, A. Coldea, D. Prabhakaran, L. R. Shelford, S. C. Speller, T. Mousavi, C. Grovenor, Z. Salman, S. R. Giblin, G. van der Laan, and T. Hesjedal, New J. Phys. **15**, 103016 (2013).

[26] G. van der Laan, B. T. Thole, G. A. Sawatzky, J. B. Goedkoop, J. C. Fuggle, J. M. Esteva, R. C. Karnatak, J. P. Remeika, and H. A. Dabkowska, Phys. Rev. B **34**, 6529 (1986).

[27] B. T. Thole, P. Carra, F. Sette, and G. van der Laan, Phys. Rev. Lett. **68**, 1943 (1992).

[28] P. Carra, B. T. Thole, M. Altarelli, and X. Wang, Phys. Rev. Lett. **70**, 694 (1993).

[29] G. van der Laan, Phys. Rev. B **57**, 112 (1998).

[30] G. van der Laan, A. I. Figueroa, and T. Hesjedal, submitted **xxx**, xxxxxx (2016).

[31] B. T. Thole, G. van der Laan, J. C. Fuggle, G. A. Sawatzky, R. C. Karnatak, and J. M. Esteva, Phys. Rev. B **32**, 5107 (1985).